Origin, synchronization, and propagation of sleep slow waves in children

Anna Castelnovo , Althea Lividini , Brady A. Riedner , Giulia Avvenuti , Stephanie G. Jones , Silvia Miano , Giulio Tononi , Mauro Manconi , Giulio Bernardi

PII: S1053-8119(23)00284-7
DOI: https://doi.org/10.1016/j.neuroimage.2023.120133
Reference: YNIMG 120133

To appear in: *NeuroImage*

Received date: 28 November 2022
Revised date: 30 March 2023
Accepted date: 21 April 2023

Please cite this article as: Anna Castelnovo , Althea Lividini , Brady A. Riedner , Giulia Avvenuti , Stephanie G. Jones , Silvia Miano , Giulio Tononi , Mauro Manconi , Giulio Bernardi , Origin, synchronization, and propagation of sleep slow waves in children, *NeuroImage* (2023), doi: https://doi.org/10.1016/j.neuroimage.2023.120133

Origin, synchronization, and propagation of sleep slow waves in children

Anna Castelnovo [1,2,3], Althea Lividini [4], Brady A. Riedner [5], Giulia Avvenuti [6], Stephanie G. Jones [7], Silvia Miano [1,2], Giulio Tononi [7], Mauro Manconi [1,2,8], Giulio Bernardi [6]

[1]Sleep Medicine Unit, Neurocenter of Southern Switzerland, Ospedale Civico, Lugano, Switzerland.

[2]Faculty of Biomedical Sciences, Università della Svizzera Italiana, Lugano, Switzerland.

[3]University Hospital of Psychiatry and Psychotherapy, University of Bern, Bern, Switzerland.

[4]Epilepsy Center - Sleep Medicine Center, Childhood and Adolescence Neuropsychiatry Unit, ASST SS. Paolo e Carlo, San Paolo Hospital, Milan, Italy

[5]Center for Sleep and Consciousness, Department of Psychiatry, University of Wisconsin - Madison, Madison, WI, USA.

[6]MoMiLab Research Unit, IMT School for Advanced Studies Lucca, Lucca, Italy.

[7]Department of Psychiatry, Wisconsin Institute for Sleep and Consciousness, University of Wisconsin-Madison, Madison, WI, USA

[8]Department of Neurology, University Hospital, Inselspital, Bern, Switzerland.

*Corresponding author: Anna Castelnovo, via Tesserete 46, 6900 Lugano, anna.castelnovo@eoc.ch; *Co-corresponding author: Giulio Bernardi, Piazza San Francesco, 19, Lucca 55100, Italy. Electronic address: giulio.bernardi@imtlucca.it.

Abstract

Study Objectives

Sleep slow wave activity, as measured using EEG delta power (<4 Hz), undergoes significant changes throughout development, mirroring changes in brain function and anatomy. Yet, age-dependent variations in the characteristics of individual slow waves have not been thoroughly investigated. Here we aimed at characterizing individual slow wave properties such as origin, synchronization, and cortical propagation at the transition between childhood and adulthood.

Methods

We analyzed overnight high-density (256 electrodes) EEG recordings of healthy typically developing children (N=21, 10.3±1.5 years old) and young healthy adults (N=18, 31.1±4.4 years old). All recordings were preprocessed to reduce artifacts, and NREM slow waves were detected and characterized using validated algorithms. The threshold for statistical significance was set at p=0.05.

Results

The slow waves of children were larger and steeper, but less widespread than those of adults. Moreover, they tended to mainly originate from and spread over more posterior brain areas. Relative to those of adults, the slow waves of children also displayed a tendency to more strongly involve and originate from the right than the left hemisphere. The separate analysis of slow waves characterized by high and low synchronization

efficiency showed that these waves undergo partially distinct maturation patterns, consistent with their possible dependence on different generation and synchronization mechanisms.

Conclusions

Changes in slow wave origin, synchronization, and propagation at the transition between childhood and adulthood are consistent with known modifications in cortico-cortical and subcortico-cortical brain connectivity. In this light, changes in slow-wave properties may provide a valuable yardstick to assess, track, and interpret physiological and pathological development.

Keywords

Development, maturation, slow wave activity, SWA, traveling

Highlights

- Slow-wave origin and distribution are more posterior and asymmetric in children than in young adults
- Slow-wave amplitude is larger and globality is lower in children than in young adults
- Slow-waves with different synchronization efficiency undergo distinct maturational changes
- The observed changes may reflect the maturation of local and long-range connections

- Slow-wave-related indices may allow to track physiological and pathological development

Introduction

During childhood and adolescence, the human brain undergoes several significant structural and functional adaptations. White-matter volume increases with age till young adulthood (Keshavan et al., 2002) according to region-specific trajectories (Lynch et al., 2020). Vice versa, starting after 7 years of age, gray matter volume declines massively and asynchronously, especially over fronto-parietal associative areas, following a posterior-anterior trajectory (Piekarski et al., 2017). This decline seems to result from the combination of selective synaptic pruning, programmed cell death, and progressive intra-cortical myelination (Paus, 2005). Importantly, a derangement of such delicate and complex processes is supposed to underlie several psychiatric disorders that typically emerge during adolescence (Paus et al., 2008).

Sleep electroencephalography (EEG) has been proposed as a reliable tool to track maturation-dependent brain adaptations occurring from infancy to young adulthood (Gorgoni et al., 2020; Ricci et al., 2021; Ringli and Huber, 2011; Schoch et al., 2018; Timofeev et al., 2020). Indeed, brain activity recorded during the sleep state is only marginally affected by confounds related to motivational, attentional, and contextual influences, thus allowing for an unbiased assessment of brain activity. Moreover, properties of sleep hallmarks such as NREM slow waves (<4 Hz) and spindles (10-16 Hz) appear to directly reflect brain organization and connectivity and may thus allow to track physiological and pathological maturational changes (Buchmann et al., 2011; Shaw et al., 2008). Sleep slow waves are especially interesting in this respect because of their dependence on short- and long-range connectivity. Specifically, local changes in synaptic strength and efficiency are thought to affect neuronal synchronization and thus slow-wave properties such as amplitude, slope, and number of negative peaks (Esser et

al., 2007; Riedner et al., 2007; Vyazovskiy et al., 2007). Differently, long-range (e.g., transcallosal) connectivity seems to affect long-range slow wave traveling at the cortical level (Avvenuti et al., 2020; Massimini et al., 2004; Murphy et al., 2009).

In line with these considerations, slow wave activity (SWA) - expressed as the mean EEG signal power within in the delta range (<4 Hz) - decreases progressively with age (Campbell and Feinberg, 2009; Jenni and Carskadon, 2004; Kurth et al., 2010), while its topographic distribution displays a shift from posterior to anterior scalp regions (Kurth et al., 2010). These changes occur in parallel with (micro)structural variations in regional myelination and cortical volume, as well as with the acquisition of region-specific skills (Kurth et al., 2012). In addition, changes in the myelination of longitudinal and interhemispheric fibers are associated with an increase in the speed and distance traveled by slow waves (Kurth et al., 2017).

Interestingly, previous work suggested the existence of at least two slow wave sub-types that are presumably generated by distinct synchronization processes (Bernardi et al., 2018; Siclari et al., 2014): 1) a likely subcortical-cortical, arousal-related process (type I) may be responsible for the emergence of widespread, large, and steep slow waves that predominate early in the falling asleep period and tend to originate from centro-frontal areas; 2) a cortico-cortical process may underlie the generation of more circumscribed, smaller, and shallower slow waves (type II) that predominate during stable NREM sleep and may originate everywhere in the cortex. The study of these slow wave sub-types across development could offer an important window on the maturation of both cortical and subcortical structures involved in sleep and slow-wave regulation.

While the above observations hint at a potential value of slow waves as markers of brain maturation, a detailed and comprehensive analysis of how topographic slow-wave characteristics and different slow-wave sub-types change from childhood to adulthood has never been performed. Notably, a better understanding of the mechanisms that regulate slow waves in relation to developmental processes could have more general implications for the use of slow waves as a marker of neurodevelopmental disorders. Indeed, the emergence of specific psychopathologies during adolescence or young adulthood has been suggested to derive from anomalies or exaggerations of typical maturation processes (Paus et al., 2008), which may be reflected in alterations of slow wave expression patterns (Tesler et al., 2013). Therefore, here we analyzed and compared night-sleep high-density EEG data (256 electrodes) collected in healthy children and young adults to investigate potential maturation-dependent changes in topographic slow-wave characteristics. In particular, we used automated methods to detect individual slow waves and analyzed their origin, regional synchronization, and propagation patterns. The following hypotheses were formulated based on known developmental brain adaptations, and on previously observed slow-wave properties. First, both slow wave origin and distribution (involvement) shift from posterior to anterior areas, thus reflecting changes in the ability of frontal areas to generate and be reached by traveling slow waves. Second, slow waves of children are less widespread and more asymmetric across the two hemispheres, as a possible consequence of an incomplete development of inter-hemispheric white-matter tracts (Bernardi et al., 2018; Siclari et al., 2014; Spiess et al., 2018). Third, different slow waves sub-types present dissociable properties and maturation patterns in line with their predominant dependence on distinct

synchronization mechanisms and brain structures (subcortical and cortical, respectively) (Bernardi et al., 2018; Siclari et al., 2014; Spiess et al., 2018).

Methods

2.1 Participants

For this observational, cross-sectional investigation, we studied healthy children and young adults recorded for one single night with the same EEG system and with similar procedures. Children were recruited at the Sleep Unit of the Civic Hospital of Lugano as control participants for a study on sleep alterations in Attention-Deficit/Hyperactivity Disorder (ADHD) (Castelnovo et al., 2022; Miano et al., 2019), while young adults were drawn from a study conducted at the University of Wisconsin-Madison sleep laboratory, as control subjects for a study evaluating the effects of meditation on sleep (Dentico et al., 2016; Ferrarelli et al., 2013).

Physicians board-certified in Sleep Medicine thoroughly interviewed children and adults to screen for any known sleep disorder, or any medical condition affecting sleep. Selected subjects were then referred to the sleep laboratory for a sleep video-PSG with extended EEG monitoring to screen for the presence of obstructive sleep apnea syndrome (OSAS) and periodic limb movements (PLM).

Selection criteria were: 1) age between 7 and 14 for the pediatric group and between 20 and 40 for the adult group; 2) negative personal history for sleep disorders; 3) good technical quality of the sleep recordings; 4) a respiratory disturbance index (RDI) < 5 events/hour.

The pediatric group was composed of 21 subjects (10.3 ± 1.5 years old, 9 females), while the adult group consisted of 18 subjects (31.1 ± 4.4, 11 females).

All study procedures were reviewed and approved by the local Independent Ethics Committee 'Comitato Etico Cantonale' (02.26.2015 – n.2881) and by the University of Wisconsin Health Sciences Institutional Review Board. All participants provided written consent upon participation. All research activities were conducted in accordance with the Helsinki Declaration.

2.2 Sleep recordings

All participants underwent an in-laboratory overnight hd-EEG recording (256 channels; Electrical Geodesics Inc., Eugene, OR) with a 250 Hz or 500 Hz sampling rate, coupled with traditional video-PSG (Berry RB, Brooks R, Gamaldo CE, Harding SM, Lloyd RM, Marcus CL, 2020). Recordings performed at 500 Hz were down-sampled to 250 Hz before data preprocessing and analysis. Lights out was within one hour of the participants most consistently reported bedtime, and wake-up time was between 6 and 7 am for all participants.

Sleep stages and sleep events were scored according to standard criteria by a board-certified sleep physician using the Embla® Remlogic Software (Neurolite), based on 30-second epochs for 6 bipolar re-referenced EEG channels (F3/M2, F4/M1, C3/M2, C4/M1, O1/M2, O2/M1), electrooculogram (EOG), and submental electromyogram (EMG) (Berry RB, Brooks R, Gamaldo CE, Harding SM, Lloyd RM, Marcus CL, 2020). Supplementary Table S1 reports the sleep macrostructure of children and adults.

2.3 EEG data preprocessing

Before spectral analysis, we pre-processed the data according to standard routines for hd-EEG. We imported all EEG signals and other relevant information (including sleep scoring), extracted NREM sleep (stages N2 and N3) epochs, and analyzed them in MATLAB (The MathWorks Inc., Natick, MA) using the EEGLAB toolbox (Delorme and Makeig, 2004). We first-order high-pass filtered at 0.1 Hz (IIR filter reproducing a single resistor capacity) and subsequently band-pass filtered the EEG signal (0.5 – 45 Hz, Kaiser window-based FIR with zero-phase distortion). An interactive open-source tool for data visualization and data-cleaning (https://github.com/CSC-UW/csc-eeg-tools.git) was used to visually inspect data in MATLAB and mark bad channels and artifactual signals. Data segments containing an arousal or movement-related artifacts affecting the majority (>50%) of all the channels were marked as 'bad' and not considered for subsequent analyses (i.e., slow waves occurring during bad segments were discarded). On average, bad segments were shorter than 30 seconds and overall represented less than 20% of the recorded NREM signal. We additionally removed channels with distinctly greater power relative to neighboring channels upon inspection of power spectra and topographic power maps. An Independent Component Analysis (ICA) was performed on N2 and N3 data separately to remove ocular (e.g., rolling eye movements), electrocardiograph, sweating, and muscular artifacts using EEGLAB routines (Delorme and Makeig, 2004). We excluded only ICA components with specific activity patterns and component maps characteristic of artifactual activity, based on the components' topographies and time series. Finally, we recovered removed bad channels using non-linear spherical interpolation.

2.4 EEG signal power in NREM sleep

Spectral analysis was performed on the average-referenced signal using artifact-free 6-second epochs (Welch's averaged modified periodogram with Hamming windows, 8 segments, 50% overlap). For topographic analyses, we computed the average delta power across epochs (SWA; 1-4 Hz) and examined both absolute and normalized power (z-score across channels, calculated using the formula $z = (x-\mu)/\sigma$, where x is the raw value for a specific electrode and μ and σ, are the mean and standard deviation computed across electrodes, respectively).

2.5 Slow wave detection

The EEG signals were referenced to linked-mastoids (right mastoid: channel 190, left mastoid: channel 94) and slow waves were detected automatically using a validated method (Bernardi et al., 2018; Siclari et al., 2014). First, we calculated the signal negative envelope by selecting for each time-point the fifth most negative sample across 191 'internal' electrodes, i.e., after exclusion of channels placed on the face and neck. This approach minimizes the risk of including in the envelope potential residual high-amplitude oscillations of artifactual origin.

We then applied a negative half-wave detection procedure based on the identification of consecutive zero-crossings on the zero-mean centered signal envelope (Vyazovskiy et al., 2007). Only half-waves with a duration of between 0.25 and 1.0 s were retained for further analyses. No amplitude thresholds were applied (Bernardi et al., 2019, 2018; Castelnovo et al., 2020, 2016; D'Agostino et al., 2018; Mensen et al., 2016; Spiess et al., 2018; Vyazovskiy et al., 2007). For all the detected slow waves, we computed and stored the following parameters of interest: duration (time between zero-crossings in seconds; s), amplitude of the maximum negative-peak (μV), down-slope (between the

first zero-crossing and the maximum negative peak; μV/s), up-slope (between the maximum negative peak and the second zero-crossing; μV/s), involvement (mean EEG signal calculated across all electrodes in a 40 ms window centered on the wave peak; μV).

2.6 Slow wave origin and propagation

For each detected slow wave, we computed its pattern of propagation by determining the topographic distribution of each local maximum negative peak relative delay (Massimini et al., 2004). We used a 'likeness constraint' method (Menicucci et al., 2009) to discard channels in which the negative wave was excessively dissimilar from a 'prototype' slow wave, defined as the wave with the largest negative peak at the time of the maximum wave peak detected on the signal negative envelope. This method is based on the cross-correlation between the instantaneous phases (estimated using the Hilbert transform) of the prototype wave and the instantaneous phases of each EEG signal (within a symmetrical 300 ms time-window) (Menicucci et al., 2009). Events falling above the 25th percentile of the distribution of the maximal cross-correlation values were retained to create a scalp delay map. Then, we applied a spatiotemporal clusterization procedure to exclude potential propagation gaps (islands of channels that likely reflect artifacts in the local EEG signal). According to this procedure, we considered the local peaks of two neighboring electrodes separated by less than 10 ms as part of the same propagation cluster. Finally, we identified the propagation cluster including the prototype wave, extracted the final delay map, and set to zero the minimum delay.

The obtained delay maps were used to compute slow-wave density, globality, probabilistic origin and termination. Specifically, slow-wave density was defined for each channel as the number of times the considered channel participated in a slow wave per minute. This index was computed in each sleep epoch after exclusion of artifactual or non-physiological activity and then averaged across epochs. Slow-wave globality was computed as the number of channels involved by individual slow waves, as extracted from the delay map. Slow-wave origin and termination were respectively defined for each slow wave as the channels showing the lowest (i.e., 0 ms) or the highest propagation delay. Thus, the probabilistic origin/termination is the percentage of slow waves that originate/terminate in each electrode.

In order to investigate whether slow waves originated with a different incidence across the two hemispheres, we classified individual slow waves as having a left (or right) hemisphere origin if 75% of the origin channels were located in the left (or right) hemisphere. Then, we determined the overall proportion of slow waves with a clear origin in the left or in the right hemisphere with respect to the total number of detected slow waves. Finally, we computed a ‘channel recruitment symmetry index’ (Avvenuti et al., 2020), defined as the number of channels in the hemisphere with less involved electrodes, divided by the total number of involved channels (%). A value of 50% indicates a symmetric distribution, while a value of 0% indicates a unilateral wave.

2.7 Principal component analysis of slow wave involvement

Previous work (Bernardi et al., 2018) used Principal Component Analysis (PCA) to investigate the possible existence of a small number of (stereotypical) scalp involvement patterns explaining most of the variance in topographic slow-wave

distribution. In adults, 95% of the variance related to slow-wave scalp involvement is explained by 3 principal components (PCs) - with maxima in the centro-frontal area (~70% of total variance), anterior or posterior areas (~20%), and left or right hemispheres (~5%) (Bernardi et al., 2018). These PCs may reflect distinct modes of slow-wave expression depending on the involvement of different wave origins or propagation patterns. Indeed, type I slow waves appeared to mainly fall into the first (centro-frontal) PC, while type II slow waves showed a more similar distribution across the three PCs. To investigate how maturational processes affect such modes of slow wave expression, here we analyzed the involvement distribution (across channels) of all slow waves using principal component analysis (PCA), as described in previous studies (Avvenuti et al., 2020; Bernardi et al., 2018). First, we confirmed through visual inspection that the same 3 main PCs observed in previous work were found in our samples of young adults and children. Then, the PC-space of each subject was rotated into a common PC space using the Procrustes transformation (Bernardi et al., 2018). The Procrustes transformation is an orthogonal transformation that minimizes the Euclidean distance between two sets of paired vectors. The reference space was selected by iteratively applying the transformation over pairs of subjects and then identifying the coordinate system (i.e., the subject) presenting the smallest distance with respect to the coordinate systems of all subjects (Haxby et al., 2011). Finally, we applied the Procrustes transformation to remap the original PC-space of each subject (adult and children subjects), into the new reference PC-space. This procedure allowed us to compare the explained variance of the PCs across individuals.

In addition, we performed source modeling of the first 100 slow waves that weighed the most on each PC using Brainstorm. For this, we selected age-appropriate MRI templates (Richards et al., 2016) segmented using the SPM12/CAT12 MATLAB toolbox (Tzourio-Mazoyer et al., 2002). A symmetric Boundary Element Model (BEM) of the head having 3 realistic layers (scalp, inner skull, outer skull)

(Maureen, 2010) and a standard co-registered set of electrode positions were used to construct the forward model. The inverse matrix was computed using the sLORETA Minimum Norm (Pascual-Marqui, 2002) with sources constrained to be perpendicular to the cortical surface and retaining only diagonal elements of the noise covariance matrix.

2.7 Slow wave synchronization

Previous work showed that, in adults, slow wave sub-types having distinct properties and regulation, and likely reflecting distinct synchronization mechanisms (type I/II), could be heuristically distinguished based on their synchronization efficiency (Bernardi et al., 2018). Specifically, a 'synchronization score' was computed for each wave as the percentage of channels showing a negative averaged current value of <-5 µV multiplied by the wave mean slope (i.e., the mean of down-slope and up-slope). Based on evidence derived from animal and computational models, this index may be expected to depend on both the number of areas/neurons contributing to the slow waves and the rapidity of their synchronization (Esser et al., 2007; Riedner et al., 2007; Vyazovskiy et al., 2007).

Here, the same approach was used to calculate the synchronization score of each detected slow wave. Then, in order to allow for interpretable comparisons between

children and adults, we selected for each participant an identical number of slow waves with high and intermediate synchronization efficiency, respectively assumed to be representative of type I and type II slow waves. From the whole distribution of synchronization scores, we identified those falling between the 90th and to the 100th percentile (top10% - putative type I), and those between the 45th and to the 55th percentile (mid10% - putative type II). We then computed the origin and scalp involvement of slow waves classified as mid10% or top10%. Involvement values of each slow wave were normalized through z-score transformation across electrodes to account for inevitable amplitude differences between slow wave sub-types. This analysis was performed only on data of the first NREM cycle to avoid possible confounds related to homeostatic changes in slow wave synchronization. Sleep cycles were defined according to the criteria proposed by Feinberg and Floyd (Feinberg and Floyd, 1979).

2.8 Statistical Analysis

Statistical between-group comparisons were performed using unpaired 2-tailed t-tests, Mann–Whitney U tests, or χ^2 tests, as appropriate. Normality of data and homogeneity of variance were first assessed using the Shapiro/Wilk's test and Levene's test, respectively. Mixed model analyses of variance (ANOVA) were used to investigate interaction effects between group (children, adult) and within-group factors.

For scalp topographic analyses, we corrected for multiple comparisons using a cluster-based method (Nichols and Holmes, 2002), as described in previous work (Castelnovo et al., 2022). Specifically, for each performed t-test, a null distribution was generated by randomly shuffling subjects across groups. At each iteration of the permutation

procedure, the test-statistics was computed for each electrode and the size of the largest significant electrode-cluster (uncorrected $p<0.05$) was stored in a frequency table. Given the impracticality of computing all possible data re-combinations, the full null distribution was approximated using 50,000 iterations. Finally, the 95th percentile (5% significance level) was used as the critical cluster-size threshold. Correlations were performed using Spearman correlation.

Alpha significance was set to $p < 0.05$. Partial Eta-squared ($\eta 2$) and Cohen's d were used as measures of effect size (Cohen, 1988). In case of non-significant results, we computed bayesian statistics (https://www.github.com/klabhub/bayesFactor), where a Bayes Factor > 3 was considered supportive for the null hypothesis.

All statistical analyses were performed in MATLAB. Data and code are only available on request via a formal request to the corresponding authors due to the need for a formal data sharing agreement.

3. Results

3.1 Slow wave activity

The children group showed higher absolute NREM SWA than the adult group over the entire scalp (cluster size = 256, $p < 0.05$; Supplementary Figure S1). After normalization, though, SWA was higher over centro-posterior regions (cluster size = 30, $p < 0.05$) and lower over frontal regions (cluster size = 69, $p < 0.05$) in the children group compared to the adult group (Supplementary Figure S1). We obtained similar

results in additional exploratory analyses focusing on N2 or N3 separately (Supplementary Figure S1), and on the first sleep cycle (*data not shown*).

3.2 Slow wave density and involvement

Absolute slow-wave density (cluster size = 158, $p < 0.05$) and involvement (cluster size = 169, $p < 0.05$) were significantly higher in children than in adults (Figure 1, Supplementary Figure S2). After normalization across electrodes, we found significantly higher values of density and involvement over posterior regions (cluster size = 72, $p < 0.05$, cluster size = 83, $p < 0.05$, respectively) and lower values over frontal regions (cluster size = 86, $p < 0.05$, cluster size = 98, $p < 0.05$, respectively) in children compared to adults. In addition, we found that slow-wave negative amplitude (2-tailed paired t-test, $p < 0.001$, $|t(1,37)| = 11.69$; $M_{children} = 73.2 \pm 10.2$, $M_{adults} = 38.8 \pm 7.7$, $M_{difference} = 34.4$, C.I. = 28.4 - 40.4, $\eta^2 = 0.79$), down-slope ($p < 0.001$, $|t(1,37)| = 7.99$; $M_{children} = 1846.6 \pm 263.4$, $M_{adults} = 1220.1 \pm 219.4$, $M_{difference} = 626.5$, CI = 467.7 - 785.5, $\eta^2 = 0.63$), and up-slope ($p < 0.001$, $|t(1,37)| = 9.66$; $M_{children} = 1620.1 \pm 206.8$, $M_{adults} = 1035.8 \pm 163.7$, $M_{difference} = 584.3$, C.I. = 461.8 - 706.8, $\eta^2 = 0.72$) were significantly higher in children compared to adults (Figure 1). On the other hand, slow-wave globality was lower in children than in adults ($p < 0.001$, $|t(1,37)| = -6.13$; $M_{children} = 31.9 \pm 1.9$, $M_{adults} = 36.9 \pm 3.1$, $M_{difference} = 6$, C.I. = -6.7 - -3.4, $\eta^2 = 0.50$). Given that slow-wave slope and globality are thought to respectively reflect short-range (Esser et al., 2007; Riedner et al., 2007; Vyazovskiy et al., 2007) and long-range (Kurth et al., 2017; Mensen et al., 2016) synchronization efficiency, we further explored the relationship between these properties in the two age groups. When adjusted for age, slow wave down-slope positively correlated with globality in adults ($p = 0.012$, $r = 0.59$), but not in children ($p =$

0.665, r = 0.10), and the correlation coefficients differed significantly between groups (p = 0.049, Fisher's z = 1.66; see Supplementary Figure S3).

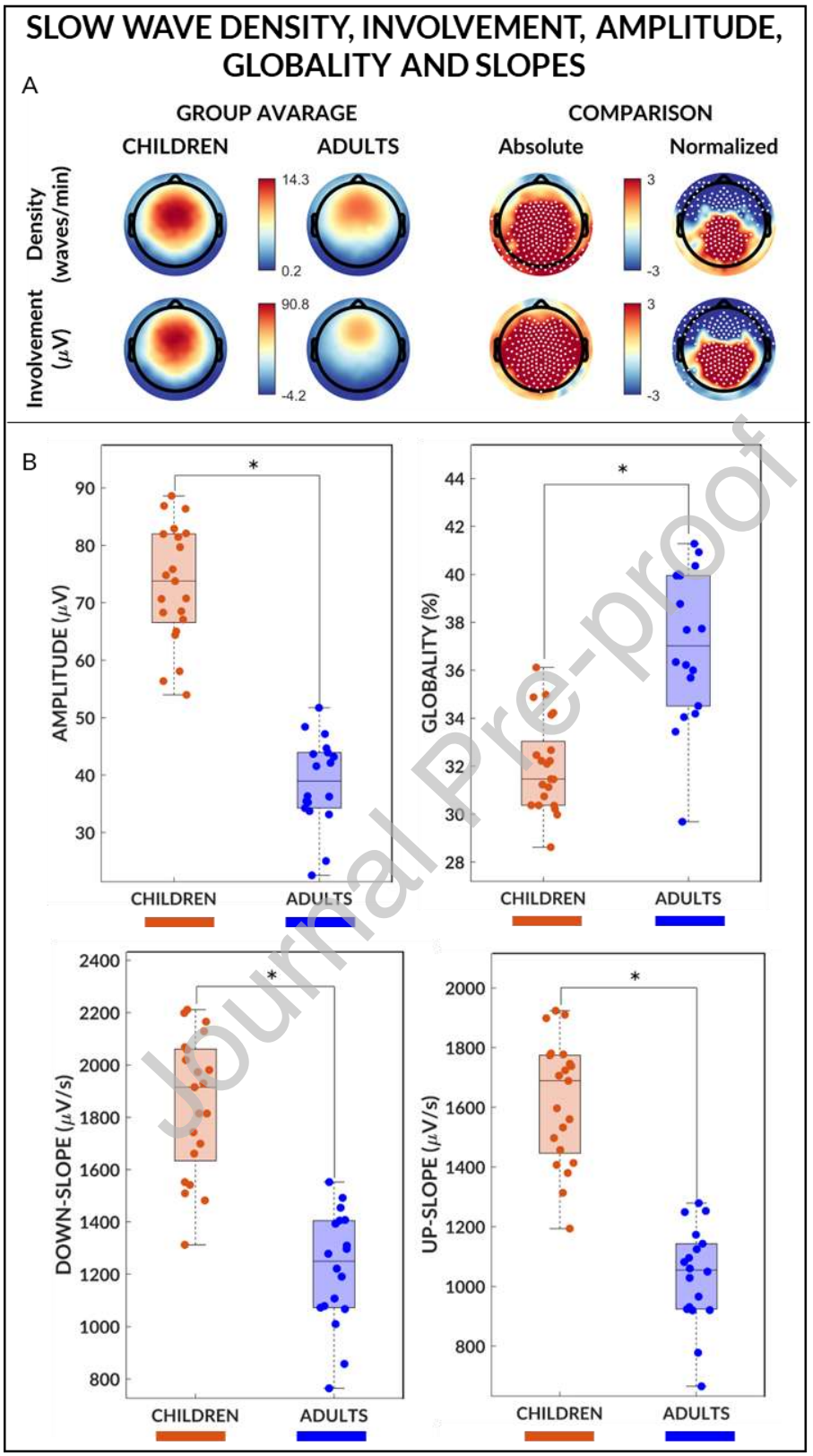

Figure 1. Slow wave density, involvement, globality, amplitude and slopes

Slow wave density and involvement were higher and distributed more posteriorly in children compared to adults. Upper panel: Slow wave density and involvement topography. Values are color coded and plotted on the planar projection of the hemispheric scalp model. First row: slow wave density (waves/minute). Second row: slow wave involvement (μV). First and second column: average values for children and adults, respectively. Higher values are shown in red, lower in blue. Third and fourth column: t-value (two-tailed, unpaired) maps for the comparison between the two groups in terms of absolute and normalized (z-score across all electrodes) values, respectively. Blue: children < adult. Red: children > adult. White circles: significant electrodes (p < 0.05, cluster-size correction).

Lower panel: Boxplots for specific slow-wave properties: top-left, maximum negative-peak amplitude *(μV); top-right, slow wave globality (%); bottom-left, down-slope (μV/s), bottom-right: up-slope (μV/s). Orange dots: children. Blue dots: adults. The bottom and top of each boxplot are the 25th and 75th percentiles of the sample, respectively. The distance between the bottom and top of each box is the interquartile range. The green line in the middle of each box is the sample median. The whiskers extending above and below each box go from the end of the interquartile range to the furthest observation. The asterisks represent statistical significance at p<0.05.*

3.3 Principal component analysis of slow wave involvement

In both children and adults, most of the variance related to slow-wave involvement was explained by 3 PCs, with maxima in the centro-frontal area (adults: 72.4%; range 63.0% - 84.0%; children: 52.2%; range 36.4% - 67.1%), anterior or posterior area (adults: 21.0%; range 12.5% - 31.2%; children: 38.5%; range, 22.5% - 55.5%), and the left or right hemisphere (adults: 6.7%, range: 3.5% - 10.6%; children: 9.3%; range, 5.4% - 11.4%), respectively (Figure 2, Supplementary Figure S4). All PCs were characterized by a maximal slow wave expression in inferior frontal and inferior temporal areas,

though they differed in terms of overall extent and relative distribution (also see Supplementary Figure S5-8).

In the children group, compared to the adult group, we observed a significant increase in the variance explained by the second (anterior/posterior: $p < 0.0001$, Cohen's $d = 2.52$) and third (left/right: $p < 0.0001$, Cohen's $d = -2.22$) PCs, at the expense of the first PC (centro-frontal: $p < 0.001$, Cohen's $d = -1.60$; Figure 2). Moreover, in children, the variance explained by the first and second PCs respectively showed a positive ($p = 0.034$, $r = 0.46$) and a negative correlation with age ($p = 0.027$, $r = -0.48$). No correlation with age was found for the third PC ($p = 0.804$, $r = 0.06$). In the adult group, none of the PCs were correlated with age (first PC: $p = 0.343$, $r = -0.237$; second PC: $p = 0.670$, $r = 0.12$; third PC: $p = 0.282$; $r = 0.27$; Figure 2).

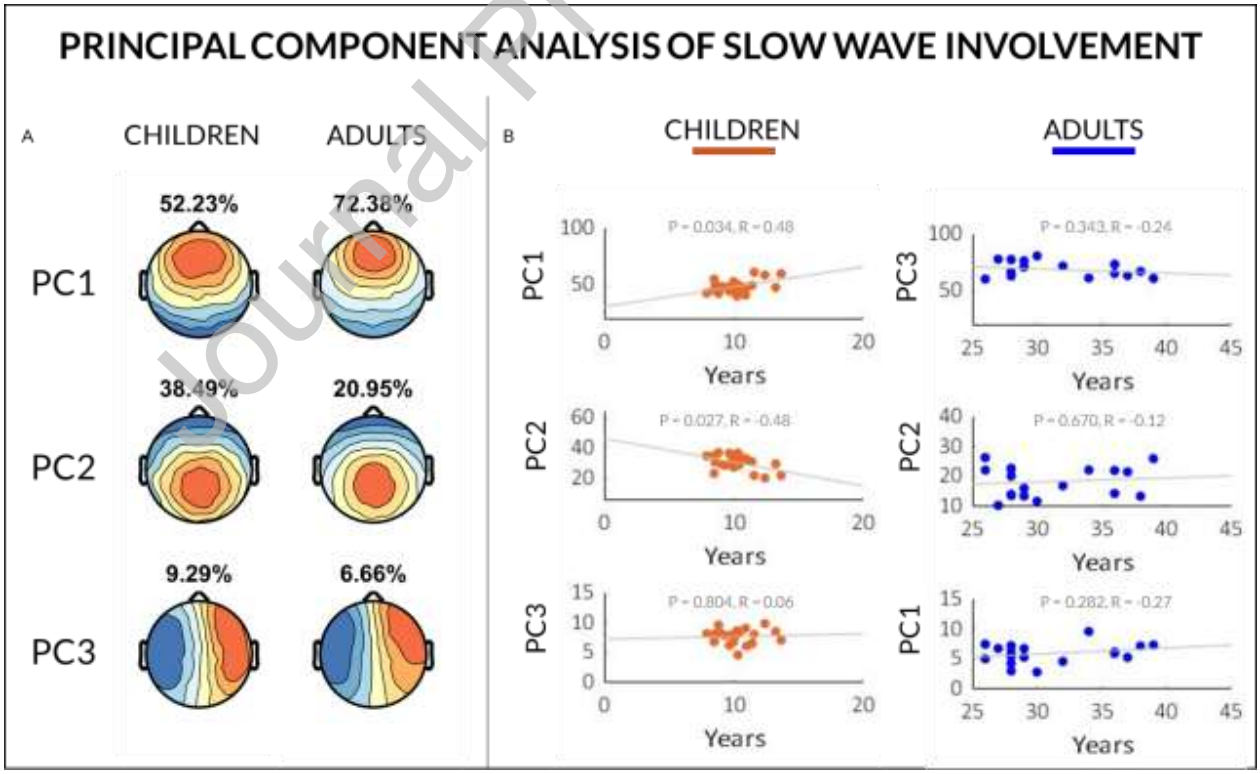

Figure 2. PC-based analysis of slow-wave involvement.

The centro-frontal (first) component was more represented in adults, while the antero-posterior (second) and left-right (third) components were more represented in children. In children, the first component was positively correlated with age, while the second component was negatively correlated with age. Left panel: The involvement distribution (mean EEG signal calculated across all electrodes in a 40 ms window centered on the wave peak) of all slow waves was entered in a PC analysis. The average variance explained is shown for each PC and group (after the Procrustes transformation computed to 'align' PCs across subjects and groups). PC1: first component; PC2: second component; PC3: third component. Right panel: correlation between age and variance explained by each PC. Orange dots: children. Blue dots: adults. Gray Line: least-squares regression line.

3.4 Recruitment symmetry index

The left-right symmetry (channel recruitment symmetry index) was significantly different between children and adults (2-tailed unpaired t-test, $p < 0.001$, $|t(1,37)| = -5.58$; $M_{children} = 29.9 \pm 1.2$, $M_{adults} = 32.4 \pm 1.6$, $M_{difference} = 2.5$, C.I.: -3.5 - -1.6, $\eta^2 = 0.65$; Figure 3). In addition, the symmetry index computed over anterior channels was significantly higher than the symmetry index computed for posterior channels in both groups (2-tailed paired t-tests; children: $p < 0.001$, $|t(20)| = 10.26$; $M_{anterior} = 28.7 \pm 1.6$, $M_{posterior} = 23.9 \pm 1.6$, $M_{difference} = 4.8\%$, C.I. = -3.8 - 5.8, $\eta^2 = 0.80$; adults: $p < 0.001$, $|t(17)| = 22.52$; $M_{anterior} = 32.3 \pm 1.8$, $M_{posterior} = 23.9 \pm 2.1$, $M_{difference} = 8.4$, C.I. = 7.6 - 9.2, $\eta^2 = 0.97$).

There was a significant interaction (Wilks-lambda = 0.51, F(1,37) = 35.49, p < 0.001, partial η^2 = 0.49) between group (children, adults) and region (anterior, posterior). Indeed, the symmetry index computed for anterior channels was higher in adults relative to children (2-tailed unpaired t-test, p <0.001, |t(1,37)| = -6.57; $M_{anterior}$ = 28.7 ± 1.6, $M_{posterior}$ = 32.3 ± 1.8, $M_{difference}$ = 3.6, C.I. = -4.7 - -2.5, η^2 = 0.72), while no statistically significant difference emerged in the symmetry index computed over posterior channels (2-tailed unpaired t-test, p = 0.932, |t(1,37)| = 0.09; $M_{anterior}$ = 23.9 ± 1.6, $M_{posterior}$ = 23.9 ± 2.1, $M_{difference}$ = 0.0, C.I. = -1.1 - 1.2, η^2 <0.01; Bayes factor = 3.17; Figure 3). Thus, anterior slow waves were more asymmetric in children relative to adults, while the degree of hemispheric asymmetry was similar across groups for posterior areas.

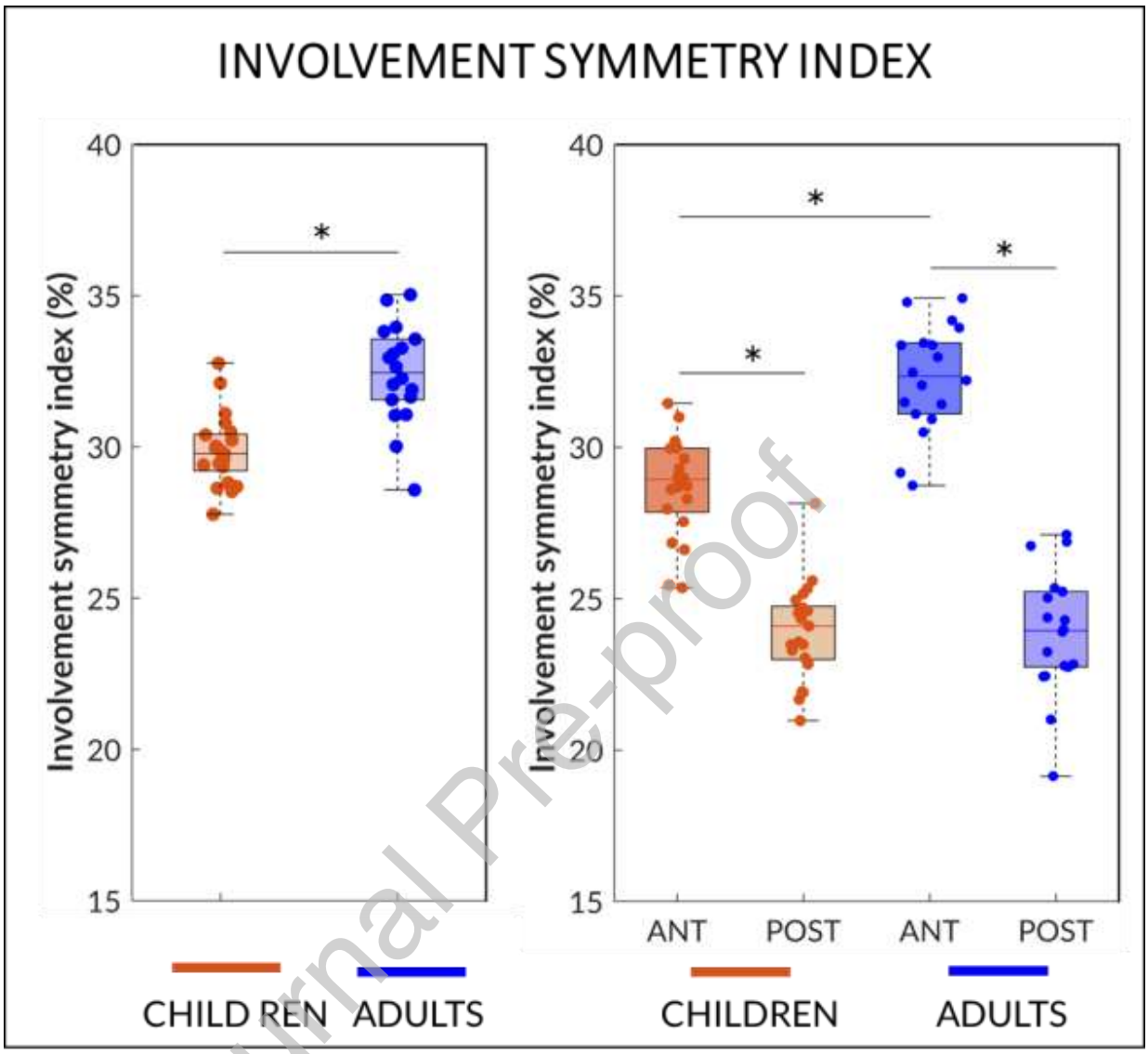

Figure 3. Slow wave channel recruitment symmetry index

Slow waves were more asymmetrically distributed in children compared to adults, especially over frontal regions. Left Panel: Symmetry index computed taking into account all channels involved in each slow wave.

Right Panel: Symmetry index computed separately for channels posterior to Cz (ANT: anterior, POST: posterior). Orange dots: children. Blue dots: adults. The bottom and top of each boxplot are the 25th and 75th percentiles of the sample, respectively. The distance between the bottom and top of each box is the interquartile range. The line in the middle of each box is the sample median. The whiskers extending

above and below each box go from the end of the interquartile range to the furthest observation. The asterisks represent statistical significance at p<0.05.

3.5 Slow-wave origin and termination

While the topographic distribution of slow-wave termination did not differ significantly between children and adults ($p > 0.05$), slow-waves appeared to originate significantly more often from frontal areas in adults relative to children (cluster size = 85, $p < 0.05$; Figure 4, Supplementary Figure S9-10). A complementary statistical trend was also observed in posterior electrodes, which showed a higher origin probability in children relative to adults ($p < 0.05$, uncorrected). In line with these observations, we found that the coordinates of the probabilistic origin peak on the anterior-posterior axis differed significantly between children and adults (2-tailed unpaired t test, $p = 0.005$, $|t(1,37)| = -3.01$; $M_{children} = 2.1 \pm 4.7$, $M_{adults} = 2.7 \pm 2.6$, $M_{difference} = 2.1$, C.I.: -4.3 - -0.8, $\eta^2 = 0.237$; Figure 4).

There was a significant interaction (Wilks-lambda = 0.87, $F(1,37) = 5.64$, $p = 0.023$, partial $\eta^2 = 0.13$) between group (children, adults) and hemispheric origin probability (left, right). In fact, the percentage of waves that originated in the right hemisphere was significantly higher than the percentage of waves that originated in the left hemisphere in children (2-tailed paired t-test, $p = 0.029$, $|t(20)| = 2.35$; $M_{left} = 43.0 \pm 3.3$, $M_{right} = 46.0 \pm 3.5$, $M_{difference} = 3.0$, C.I. = -0.3 - 5.6, $\eta^2 = 0.22$) but not in adults ($p = 0.386$, $|t(17)| = -0.89$, $M_{left} = 43.3 \pm 6.0$, $M_{right} = 42.7 \pm 5.8$, C.I. = -2.0 - 0.8, $M_{difference} = 0.6$, partial $\eta^2 = 0.04$). The percentage of slow waves that originated in the right hemisphere was higher in children compared to adults (2-tailed unpaired t-test, $p = 0.040$, $|t(20)| =$

2.13; $M_{children}$ = 45.7 ± 3.5, M_{adults} = 42.5 ± 3.3, $M_{difference}$ = 3.2, C.I. = -0.2 - 6.3, η^2 = 0.19), while the percentage of slow waves that originated in the left hemisphere did not statistically differ between groups ($p = 0.827$, $|t(17)| = -0.22$; $M_{children}$ = 28.7 ± 1.6, M_{adults} = 23.9 ± 1.6, $M_{difference}$ = 0.33, C.I. = -3.4 - 2.7, $\eta^2 < 0.01$, Bayes factor = 3.135; Figure 4).

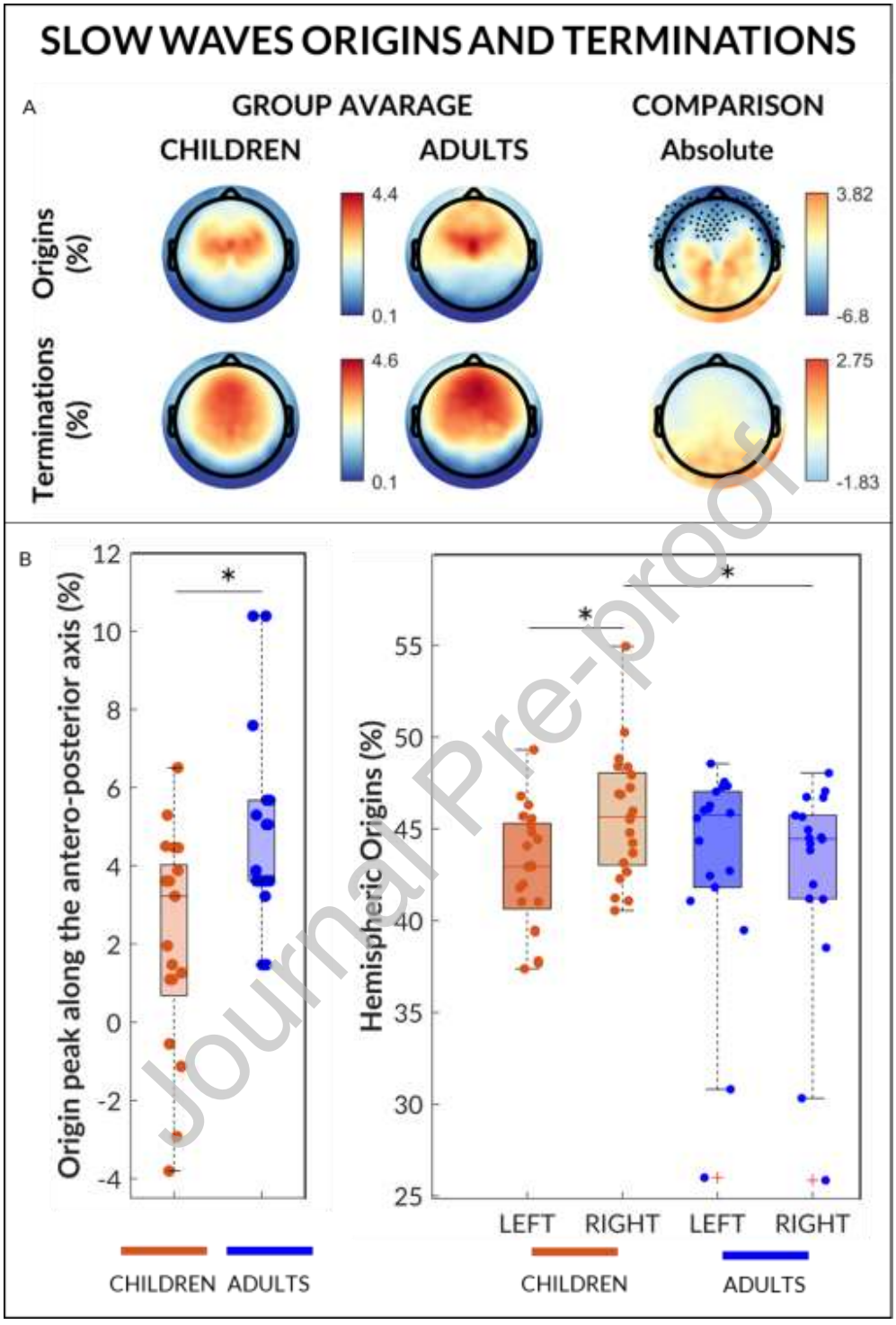

Figure 4. Slow wave origins and terminations

Slow-wave origin (but not termination) probability was lower over frontal regions and higher in the right hemisphere in children compared to adults. Upper panel: Slow wave origin and termination. Values are

color coded and plotted on the planar projection of the hemispheric scalp model. First row: distribution of slow-wave origins (% of the total). Second row: distribution of slow wave terminations (% of the total). First and second columns: average values for the children group and the adult group, respectively. Higher values are shown in red, lower in blue. Third column: t-value (two-tailed, unpaired) maps for the comparison between the two groups. Blue: children < adult. Red: children > adult. White circles: significant electrodes ($p < 0.05$, cluster-size correction).

Lower panel: Slow-wave origin distribution along the antero-posterior axis (left lower panel) and in the right compared to the left hemisphere (right lower panel). Orange dots: children. Blue dots: adults. The bottom and top of each boxplot are the 25th and 75th percentiles of the sample, respectively. The distance between the bottom and top of each box is the interquartile range. The line in the middle of each box is the sample median. The whiskers extending above and below each box go from the end of the interquartile range to the furthest observation within the whisker length. Observations beyond the whisker length (more than 3 times the interquartile range away from the bottom or top of the box) are marked as outliers (red crosses). The asterisks represent statistical significance at $p<0.05$.

3.6 Slow waves with high and low synchronization efficiency

For each slow wave, a synchronization score was computed based on the mean slope and proportion of involved electrodes, as a measure of slow-wave synchronization efficiency. The synchronization score distribution was non-Gaussian and right skewed in both groups (Figure 5). However, on average, children had higher synchronization scores (Median = 1.6, range = 0.3 - 4.5) compared to adults (Median = 0.9, range = 1.3 - 2.2; Mann-Whitney U Test, $z = -5.23$, $U = 174$, $p < 0.01$, $\eta^2 = 0.848$). The synchronization score distributions remained similar across NREM cycles, but also showed a clear leftward shift compatible with the effects of homeostatic changes in slow-wave amplitude and globality (Figure 5). Thus, to avoid possible confounds related to homeostatic changes, we focused further analyses on the first NREM cycle only. We

then classified and separately analyzed slow waves with high (top10%) and intermediate (mid10%) synchronization efficiency.

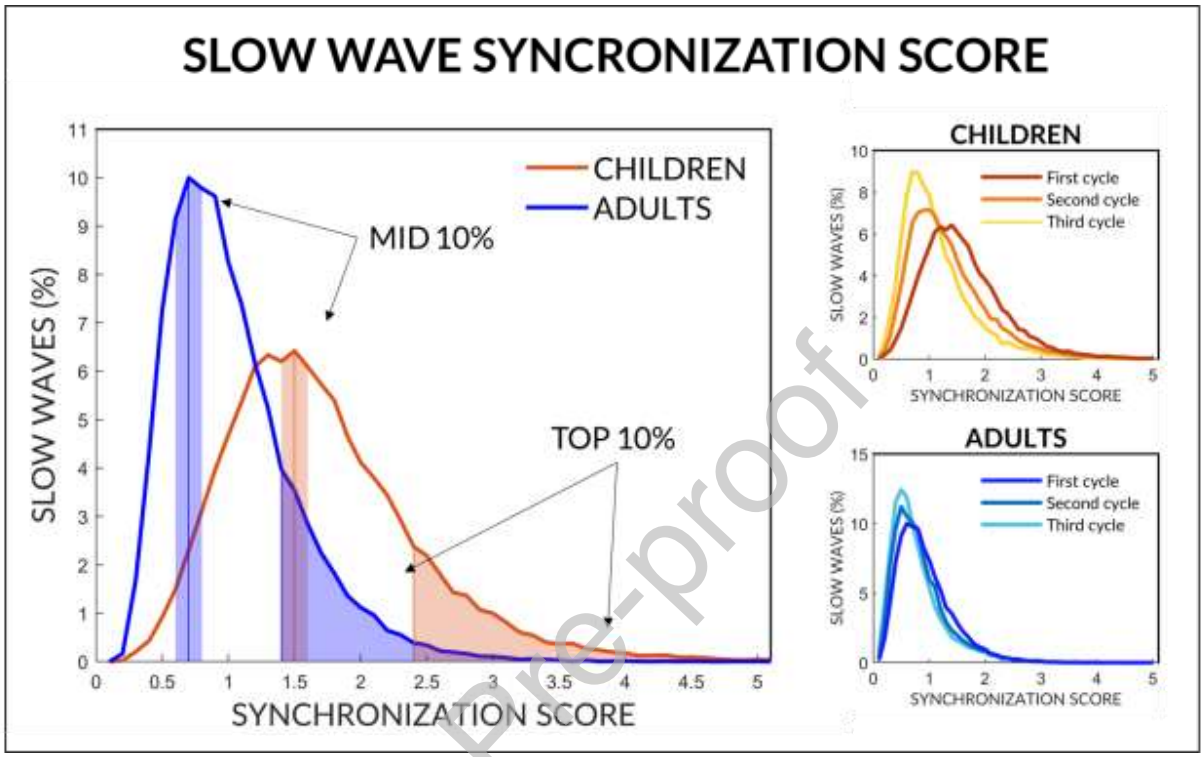

Figure 5. Slow wave synchronization score

Slow-wave synchronization efficiency was higher in children compared to adults. In both groups, slow wave synchronization decreased across sleep cycles. Left panel: The two curves represent the distribution of synchronization scores (group average) during the first NREM sleep cycle in children (orange) and adults (blue). Right panels: The three curves represent the average distribution of synchronization scores during the first, second and third NREM sleep cycle in children (upper right panel) and adults (right lower panel).

Given that slow waves were classified based on their slope and globality, we first analyzed the relative contribution of these two parameters to synchronization efficiency (Supplementary Figure S11). We found no significant interaction between group

(children, adults) and slow-wave sub-type (mid10%, top10%) for globality (Wilks-lambda = 0.99, F(1,37) = 0.47, p = 0.499, partial η^2 = 0.01, Bayes factor for the difference between top% and mid10% in adults and in children = 2.660). However, we identified a significant main effect of group (F(1,37) = 21.65, p < 0.001, partial η^2 = 0.37) indicating that slow waves were overall more global in adults compared to children, and a main effect of wave sub-type (Wilks- lambda = 0.11, F(1,37) = 301.16, p < 0.001, partial η^2 = 0.89), with both groups showing more global top10% slow waves than mid10% slow waves.

We then analyzed slow-wave down-slope and found a significant interaction (Wilks-lambda = 0.70, F(1,37) = 37.00, p < 0.001, partial η^2 = 0.30) between group (children, adults) and slow wave sub-type (mid10%, top10%). We also found a main effect of group (F(1,37) = 84.45, p < 0.001, partial η^2 = 0.696), indicating that slow waves were overall steeper in children compared to adults (top10%: p <0.001, |t(37)| = -8.74; $M_{children}$ = 2981.5 ± 434.5, M_{adults} = 1873.6 ± 342.3, C.I. = -1364.8 - -850.9, η^2 = 0.68; mid10%, p <0.001, |t(37)| = -8.35; M_{adults} = 1210.3 ± 225.0, $M_{children}$ = 1973.6 ± 327.0, C.I.= -948.59 - -578.01, η^2 = 0.65), and a main effect of slow-wave sub-type (Wilks-lambda = 0.090, F(1,37) = 375.46, p < 0.001, partial η^2 = 0.91), with both the adult (2-tailed paired t-test, p <0.001, |t(17)| = 11.53, C.I. = 542.0 - 784.7, η^2 = 0.88) and the children (tailed paired t-test, p <0.001, |t(20)| = 16.06, C.I. = 876.9 - 1138.8, η^2 = 0.93) groups showing steeper top10% than mid10% slow waves.

Slow waves with high and intermediate synchronization efficiency were then analyzed and compared for probabilistic origin and normalized scalp involvement (Figure 6). Both mid10% and top10% slow waves had a more posterior involvement in children than in

adults. We found a significant interaction between group (children, adults) and wave type (mid10%, top10%) for normalized involvement in a frontal (63 channels, $p < 0.05$) and a parieto-occipital cluster (77 channels, $p < 0.05$, Figure 6). Specifically, adults had higher involvement values compared to children in the frontal cluster for both top10% (2-tailed unpaired t-test, $p < 0.001$, $|t(37)| = 7.47$; $M_{children} = 0.4 \pm 0.2$, $M_{adults} = 0.8 \pm 0.1$, C.I. = 0.1 - 0.2, $\eta^2 = 0.60$) and mid10% slow waves (2-tailed paired t-test, $p < 0.001$, $|t(37)| = 6.17$; $M_{right} = 0.4 \pm 0.1$, $M_{adults} = 0.6 \pm 0.1$, C.I. = 0.3 - 0.5, $\eta^2 = 0.51$). Moreover, adults displayed significantly higher involvement values for top10% compared to mid10% slow waves within the same cluster ($p < 0.001$, $|t(17)| = 5.20$; C.I. = 0.1 - 0.2, $\eta^2 = 0.615$), while no statistical difference emerged in children ($p = 0.120$, $|t(20)| = -1.62$; C.I. = -0.1 - 0.0, $\eta^2 = 0.11$; Bayes factor = 1.425; Figure 6C). Similar differences - though opposite in sign - were found in the posterior cluster (Supplementary Figure S11).

Both mid10% and top10% slow waves showed a tendency to originate from central and frontal electrodes, but a clear origin hot-spot was evident only for top10% slow waves of adults. We found a significant interaction between group and wave sub-type for slow-wave probabilistic origin in a central cluster of electrodes (14 channels, $p < 0.05$, Figure 6). Post-hoc analyses showed that, within this cluster, adults had a higher origin probability compared to children for top10% (2-tailed unpaired t-test, $p < 0.001$, $|t(37)| = 4.81$; $M_{children} = 3.0 \pm 1.1$, $M_{adults} = 4.9 \pm 1.3$, C.I. = 1.1 - 2.6, $\eta^2 = 0.46$) but not for mid10% slow waves ($p = 0.971$, $|t(37)| = -0.04$; $M_{children} = 3.0 \pm 0.9$, $M_{adults} = 3.0 \pm 0.8$, C.I. = -0.6 - 0.5, $\eta^2 < 0.01$, Bayes Factor = 3.18). Moreover, adults were characterized by a significantly higher origin probability for top10% than mid10% slow waves within

the same electrode cluster ($p < 0.001$, $|t(20)| = 6.30$, C.I. = 1.2 - 2.5, $\eta^2 = 0.67$). A similar difference was not found in children ($p = 0.935$, $|t(20)| = -0.08$; C.I. = -0.5 - 0.4, $\eta^2 < 0.01$, Bayes factor = 3.010; Figure 6, Supplementary Figures S12-13).

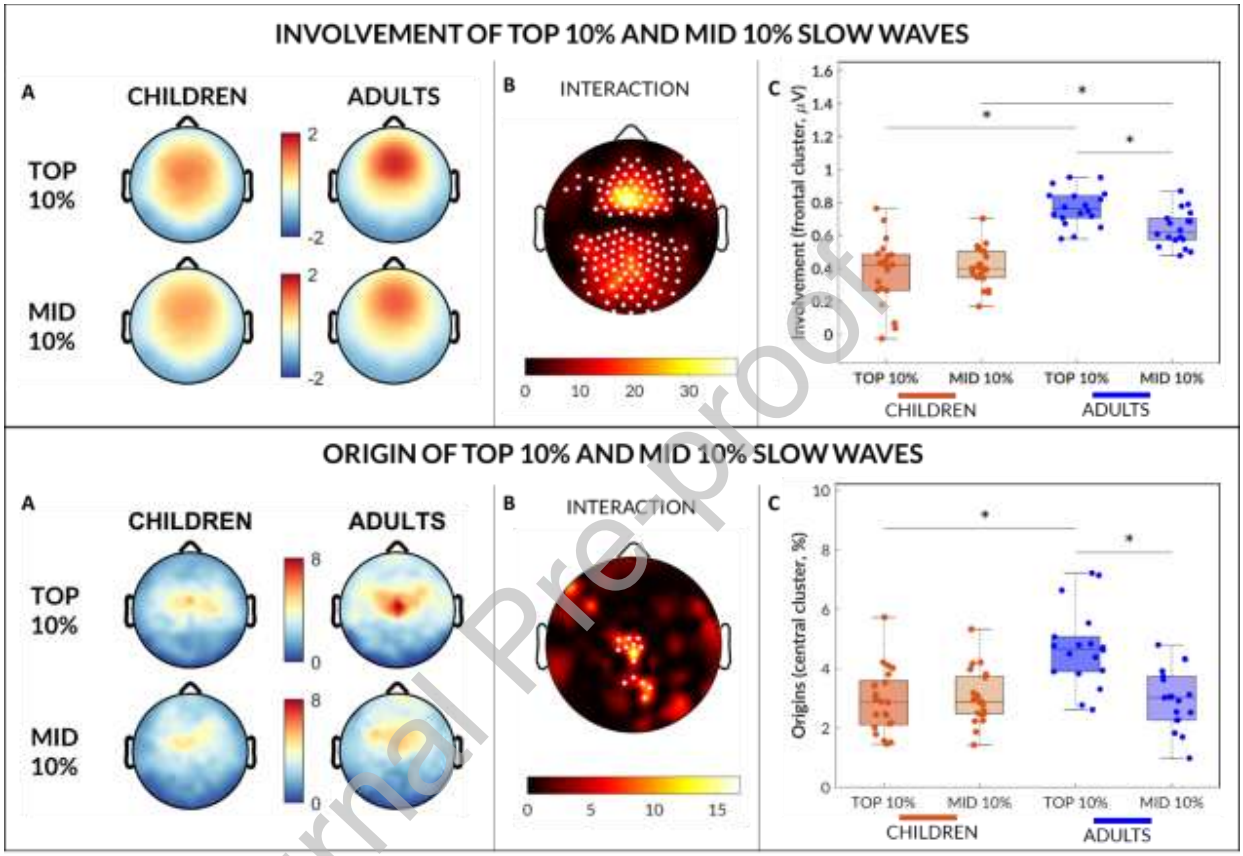

Figure 6. Origin and involvement of slow waves with high and intermediate synchronization efficiency

Type I slow-waves in adults were distributed more frontally and originated more consistently over a central cluster of electrodes compared to type II slow waves in adults and both type I and type II slow waves in children. Slow-wave origin: channels showing zero propagation delay. Slow wave involvement: mean EEG signal in a 40-ms window around the wave peak. Involvement (top) and origin (bottom) of slow waves with high (top10%) and intermediate (mid10%) synchronization scores. Values are color coded and plotted on the planar projection of the hemispheric scalp model. Top10% slow waves of adults displayed a more frontal distribution compared to mid10% slow waves and both top10% and mid10% slow waves of children.

A| Topographic analysis - Average distribution of involvement/origin values for slow waves with high (top10%; first row) and intermediate (mid10%; second row) synchronization efficiency. Higher values are shown in red, lower in blue.

B| Interaction effect of the mixed-model within/between groups ANOVA. Lower F-values are represented in dark-red/black, while higher F- values in yellow/white. White circles indicate significant electrodes ($p < 0.05$, cluster-size correction).

C| Dots represent the average of channels within significant clusters of electrodes in Figure B (as two clusters were significant for the involvement, only the frontal cluster is represented here, while the posterior cluster is represented in Supplementary Figure 12). Orange dots: children; blue dots: adults. The bottom and top of each boxplot are the 25th and 75th percentiles of the sample, respectively. The distance between the bottom and top of each box is the interquartile range. The line in the middle of each box is the sample median. The whiskers extending above and below each box go from the end of the interquartile range to the furthest observation within the whisker length. The asterisks represent statistical significance at $p<0.05$.

Discussion

In the present study, we examined changes in slow-wave origin, synchronization and propagation from childhood to early adulthood using sleep hd-EEG. We found that, from childhood to adulthood: i) both the origin and topographic distribution of slow waves move towards more anterior brain regions; ii) slow waves become more global and more symmetric across hemispheres; iii) slow waves characterized by intermediate and high synchronization efficiency (putative type I and type II slow waves) display partially dissociated maturational changes.

Slow wave origin and involvement become more anterior from childhood to adulthood

Previous work demonstrated a progressive anteriorization of the SWA (delta power) peak during normal development (Kurth et al., 2010). Such a change has been suggested to reflect a relative variation in inter-regional slow wave synchronization/propagation related to the maturation of frontal brain areas and their connectivity. More recently, preliminary observations suggested that the regional propensity to generate slow waves might also change following a posterior-to-anterior gradient from childhood to adulthood (Timofeev et al., 2020). Consistent with previous data, our present results show that both slow wave cortical distribution (involvement) and tendency to generate slow waves (origin) are stronger in anterior areas in young adults relative to children. In addition, our PCA-based analysis revealed that slow-wave scalp topography tends to follow a specific set of patterns that is common to both children and adults, and that the relative 'weight' of these patterns changes across development. Indeed, regardless of age, 95% of the variance related to slow wave involvement can be explained by 3 PCs, with maxima located in the central-frontal area, anterior or posterior areas, and left or right hemispheres (Bernardi et al., 2021). However, the relevance of the central-frontal PC appears to increase from childhood to adulthood at the expense of the other two PCs. These observations suggest that while most slow waves of children and adults may involve specific, partly overlapping brain networks, their relative propensity to 'reach' more anterior areas changes during development.

Together, our results indicate that in children, frontal areas have a lower propensity at both generating and being crossed by slow waves originating elsewhere relative to what is commonly observed in adults. Such modifications could reflect partially distinct maturational processes, such as local changes in microstructural organization and modifications in long-range connectivity, respectively (Spiess et al., 2018).

Slow wave interhemispheric asymmetry is more pronounced in children than in adults

The PCA-based analysis and the inter-hemispheric involvement analyses revealed that slow waves of children are characterized by a greater tendency to remain unilateral or at least more asymmetric on the left-right axis than slow waves of adults. Moreover, the involvement asymmetry was found to be stronger in anterior than in posterior areas.

Previous work showed that the degree of cross-hemispheric slow-wave propagation directly depends on the existence and integrity of interhemispheric (callosal) connections. Indeed, slow waves (but not spindles) of callosotomized epileptic adult patients typically remain circumscribed to the brain hemisphere in which they originate, while this is relatively uncommon in non-callosotomized individuals (Avvenuti et al., 2020; Bernardi et al., 2021). Based on this observation, our present results could be explained by an incomplete maturation of the corpus callosum in children (Giedd et al., 1999; Luders et al., 2010b). In fact, the size of the corpus callosum is known to increase throughout adolescence and up to the middle 20s (Keshavan et al., 2002), following a posterior-to-anterior gradient of maturation (Danielsen et al., 2020; Giedd et al., 1999;

Luders et al., 2010a; Rajapakse et al., 1996; Thompson et al., 2000; Westerhausen et al., 2016) .

In addition, here we found in children (and not in adults) a significant interhemispheric origin asymmetry, with more slow waves originating in the right than in the left hemisphere. This is, again, consistent with findings obtained in callosotomized patients. Indeed, while previous work observed a tendency for slow waves to originate more often in the right than in the left hemisphere in both non-callosotomized and callosotomized individuals, the asymmetry appeared to be stronger in the latter group (Bernardi et al., 2021). Interestingly, this effect could depend on an accentuation of otherwise small physiological asymmetries related to (micro)structural or functional factors due to a reduction in the synchronization between the two hemispheres. For instance, previous evidence indicates that the human brain may show lower SWA in the left than in the right hemisphere during the first night spent in a new environment (Tamaki et al., 2016), reminiscing the monitoring function of unihemispheric sleep in migratory birds and aquatic mammals (Mascetti, 2016). This relative asymmetry might become more pronounced when the coordination of activity between hemispheres is reduced. Alternatively, the observation of stronger origin asymmetries in individuals with an immature or absent corpus callosum could have a methodological explanation. Indeed, the reduced cross-hemispheric propagation in these individuals may lead to a more accurate localization of slow wave origin in the presence of EEG volume conduction. However, other explanations not involving the corpus callosum cannot be ruled out based on our current data. Indeed, for instance, previous work described an asymmetric maturation of higher-order association cortices that may contribute

explaining our results (Gogtay et al., 2004). Future investigation should combine the assessment of electrophysiological and brain structural changes to determine specific mechanisms underlying slow-wave asymmetries in children.

Slow waves are larger but less widespread in children than adults

Consistent with findings indicating that slow waves of children are more often asymmetrical or even unihemispheric in children than in adults, we found that the number of channels involved by each slow wave (i.e., globality) is on average smaller in children. Therefore, while slow waves of children are typically larger and steeper than those of adults, they are also less widespread (Kurth et al., 2017; Mensen et al., 2016). In addition, we found that slope and globality are positively correlated in adults but not in children, indicating a dissociation between these slow-wave properties early during development.

We hypothesize that slow-wave slope and globality may reflect the (partially) independent maturation of local and long-range connectivity, respectively. Indeed, slow-wave slope is regarded as an electrophysiological marker for neuronal synchronization speed, which is in turn thought to depend on regional synaptic strength (Esser et al., 2007; Riedner et al., 2007; Vyazovskiy et al., 2007). On the other hand, slow-wave globality likely reflects the efficacy of cortico-cortical spreading, being directly related to traveled distance (Kurth et al., 2017). Thus, slow waves of children may be locally more synchronous due to a still incomplete synaptic pruning and refinement (and thus, greater synaptic strength (Kurth et al., 2010), but they are globally less widespread, due

to an immature white matter connectome. This interpretation is consistent with the previously described correlation between distance traveled by slow waves and myelin content in whole-brain/interhemispheric connections, and between cortical involvement and myelin content in the superior longitudinal fascicle (Kurth et al., 2017). Moreover, our results are in line with the observation of an age-dependent increase in different functional and structural connectivity measures. For example, intra and inter-hemispheric delta and theta EEG coherence (a connectivity measure that was proposed to reflect white matter connectivity and myelination) (Kurth et al., 2013), as well as approximate entropy (an information-based connectivity measure) (Lee et al., 2013), positively correlate with age. Furthermore, local resting state functional connectivity decreases with age as longer connections are formed (Kelly et al., 2009; Lopez-Larson et al., 2011), with a progressive increase in the strength of functional connectivity and in the extent of functionally connected regions (Jolles et al., 2011).

Maturation of slow wave synchronization processes from childhood to adulthood

Previous work demonstrated in adults that the transition to sleep is characterized by at least two main phases: i) an early phase dominated by large and widespread (type I) slow waves (likely including classically defined K-complexes) that originate around somatic sensory-motor areas and peak in frontal regions, and ii) a late phase characterized by the predominance of shallow, local (type II) slow waves that show variable origin and distribution (Siclari et al., 2014). This temporal dissociation was suggested to reflect the existence of distinct synchronization processes - an efficient, subcortical-cortical process and a less efficient cortico-cortical process - that come into

play at different moments of the wake-sleep transition. Importantly, though, recent work revealed that the temporal dissociation between synchronization processes I and II at sleep onset is absent in children (Spiess et al., 2018). In line with this, here we found that slow waves characterized by a high synchronization efficiency (putative type I) do not present in children the same origin and distribution as those of adults. Specifically, putative type I slow waves of children do not present a clear origin hotspot in centro-frontal electrodes typically observed in adults and have a predominantly posterior rather than anterior involvement. In other words, while larger, steeper, and more global than most slow waves, highly synchronous slow waves of children are virtually indistinguishable in terms of origin and involvement from most other (type II) slow waves.

Overall, the above observations indicate that the process underlying the synchronization of type I slow waves might be largely immature in children. This conclusion is in line with previous evidence indicating that K-complexes, after their appearance at ~6 months of age, continue their maturation during childhood and reach their 'adult shape' only during adolescence (Spiess et al., 2018). Of note, while the origin and synchronization of type I slow waves is thought to be mediated by diffuse subcortico-cortical projections from arousal-related structures (Siclari et al., 2014), their cortical spreading may still depend on the state and integrity of cortico-cortical connections. Therefore, in children, a relative immaturity of arousal-related structures or their connections to the cortex might explain the lack of a well-defined origin hot-spot as found in adults (Lynch et al., 2020), while the incomplete maturation of frontal connectivity may determine a preferential propagation to posterior areas (Gogtay et al., 2004).

From a more general perspective, our results suggest that previous evidence indicating a centro-frontal origin for NREM slow waves (Avvenuti et al., 2020; Bernardi et al., 2019; Massimini et al., 2004; Menicucci et al., 2009; Murphy et al., 2009) was actually driven for the most part, if not exclusively, by type I waves. Indeed, type I slow waves appear to have a more stereotyped origin and propagation pattern relative to type II slow waves, and their 'contribution' may thus emerge upon averaging even if they represent a relatively small percentage of all slow waves.

Limitations

Some limitations of our study are worth noting. The observational and cross-sectional nature of our study does not allow us to prove causality or exclude mediating factors between age and slow wave properties, nor to show the development of EEG activity, which would require a longitudinal investigation. The lack of brain structural measurements also prevented us from investigating specific associations between EEG and brain and white matter changes. Furthermore, the children group age range was relatively limited (7-14 years old). As cortical development starts in the first years of life (Novelli et al., 2016), studying younger children will add crucial information on the link between slow-wave changes and cortical maturation. Finally, it should be noted that the two studied samples were taken from the control groups of different studies conducted in two different sleep centers. Nevertheless, all recordings were collected using the same EEG system and following the same acquisition, preprocessing, and analysis procedures.

Conclusions and future directions

Taken together, present results indicate that a detailed characterization of slow-waves properties may offer valuable information regarding morpho-functional brain adaptations across childhood and adolescence that extend and complement those derived from the simple assessment of SWA (delta power). In addition, we provide evidence supporting the existence of at least two slow-wave sub-types characterized by different levels of synchronization efficiency, and show that these waves undergo partially distinct maturational changes. In light of previous observations indicating that the generation of such slow-wave subtypes may depend respectively on subcortico-cortical and cortico-cortical synchronization mechanisms, our present results suggest that their separate assessment could offer a valuable readout regarding the maturation of distinct anatomo-functional brain networks.

Overall, the present data support the view that sleep constitutes a unique window for observing and tracking brain physiological adaptations and their disruption and contribute to the efforts aimed at providing an accurate yardstick to assess pathological development in clinical populations. Indeed, for instance, specific changes of distinct slow-wave sub-types could be linked to (and thus, track) alterations of particular brain structures or networks in pathological conditions. In this respect, alterations in the maturation of type I waves, which are supposed to reflect the involvement of ascending, arousal-related systems, may especially occur in conditions presenting functional alterations of such structures.

Acknowledgements

The authors are grateful to Giacomo Handjaras for his help in the definition of data analysis methodologies.

Funding sources

This study was in part supported by the ABREOC (Advisory Board of Scientific Research of the Ente Ospedaliero Cantonale, protocol EOC.NSI.14.12), and in part by the NCCAM (National Center for Complementary and Alternative Medicine, protocol P01AT004952. The funders had no involvement in study design, in the collection, analysis, and interpretation of data or in writing of the report and the decision to submit the article for publication.

Disclosure Statement

Declarations of interest: none

Author contributions

AC: Conceptualization; Data curation; Formal analysis; Investigation; Methodology; Writing - original draft; Software; Validation; Visualization; Project administration. AL: Data curation; Writing - review & editing. BR: Writing - review & editing; Methodology. GA: Writing - review & editing; Methodology. SGJ: Writing - review & editing. SM: Writing - review & editing; Funding acquisition. GT: MM: Writing - review & editing;

Funding acquisition. MM: Writing - review & editing; Resources. GB: Conceptualization; Methodology; Writing - review & editing; Software; Supervision.

References

Avvenuti, G., Handjaras, G., Betta, M., Cataldi, J., Imperatori, L.S., Lattanzi, S., Riedner, B.A., Pietrini, P., Ricciardi, E., Tononi, G., Siclari, F., Polonara, G., Fabri, M., Silvestrini, M., Bellesi, M., Bernardi, G., 2020. Integrity of Corpus Callosum Is Essential for theCross-Hemispheric Propagation of Sleep Slow Waves:A High-Density EEG Study in Split-Brain Patients. J Neurosci 40, 5589–5603. https://doi.org/10.1523/JNEUROSCI.2571-19.2020

Bernardi, G., Avvenuti, G., Cataldi, J., Lattanzi, S., Ricciardi, E., Polonara, G., Silvestrini, M., Siclari, F., Fabri, M., Bellesi, M., 2021. Role of corpus callosum in sleep spindle synchronization and coupling with slow waves. Brain Commun 3, fcab108. https://doi.org/10.1093/braincomms/fcab108

Bernardi, G., Betta, M., Cataldi, J., Leo, A., Haba-Rubio, J., Heinzer, R., Cirelli, C., Tononi, G., Pietrini, P., Ricciardi, E., Siclari, F., 2019. Visual imagery and visual perception induce similar changes in occipital slow waves of sleep. J Neurophysiol 121, 2140–2152. https://doi.org/10.1152/JN.00085.2019

Bernardi, G., Siclari, F., Handjaras, G., Riedner, B.A., Tononi, G., 2018. Local and Widespread Slow Waves in Stable NREM Sleep: Evidence for Distinct Regulation Mechanisms. Front Hum Neurosci 12. https://doi.org/10.3389/FNHUM.2018.00248

Berry RB, Brooks R, Gamaldo CE, Harding SM, Lloyd RM, Marcus CL, V.B., 2020. The AASM Manual for the Scoring of Sleep and Associated Events: Rules, Terminology and Technical Specifications, 2.6 versio. ed.

Buchmann, A., Kurth, S., Ringli, M., Geiger, A., Jenni, O.G., Huber, R., 2011. Anatomical markers of sleep slow wave activity derived from structural magnetic resonance images. J Sleep Res 20, 506–513. https://doi.org/10.1111/J.1365-2869.2011.00916.X

Campbell, I.G., Feinberg, I., 2009. Longitudinal trajectories of non-rapid eye movement delta and theta EEG as indicators of adolescent brain maturation. Proc Natl Acad Sci U S A 106, 5177–5180. https://doi.org/10.1073/PNAS.0812947106

Castelnovo, A., Lividini, A., Bernardi, G., Pezzoli, V., Foderaro, G., Ramelli, G.P., Manconi, M., Miano, S., 2022. Sleep Power Topography in Children with Attention Deficit Hyperactivity Disorder (ADHD). Children (Basel) 9. https://doi.org/10.3390/CHILDREN9020197

Castelnovo, A., Riedner, B.A., Smith, R.F., Tononi, G., Boly, M., Benca, R.M., 2016. Scalp and Source Power Topography in Sleepwalking and Sleep Terrors: A High-Density EEG Study. Sleep 39, 1815–1825. https://doi.org/10.5665/sleep.6162

Castelnovo, A., Zago, M., Casetta, C., Zangani, C., Donati, F., Canevini, M., Riedner, B.A., Tononi, G., Ferrarelli, F., Sarasso, S., D'Agostino, A., 2020. Slow wave oscillations in Schizophrenia First-Degree Relatives: A confirmatory analysis and feasibility study on slow wave traveling. Schizophr Res 221, 37–43. https://doi.org/10.1016/J.SCHRES.2020.03.025

Cohen, J., 1988. Statistical power analysis for the behavioral sciences, rev. ed, Cohen, Jacob. New York, NY: Academic Press.

D'Agostino, A., Castelnovo, A., Cavallotti, S., Casetta, C., Marcatili, M., Gambini, O., Canevini, M., Tononi, G., Riedner, B., Ferrarelli, F., Sarasso, S., 2018. Sleep endophenotypes of schizophrenia: slow waves and sleep spindles in unaffected first-degree relatives. NPJ Schizophr 4, 2. https://doi.org/10.1038/s41537-018-0045-9

Danielsen, V.M., Vidal-Piñeiro, D., Mowinckel, A.M., Sederevicius, D., Fjell, A.M., Walhovd, K.B., Westerhausen, R., 2020. Lifespan trajectories of relative corpus callosum thickness: Regional differences and cognitive relevance. Cortex 130, 127–141. https://doi.org/10.1016/J.CORTEX.2020.05.020

Delorme, A., Makeig, S., 2004. EEGLAB: An open source toolbox for analysis of single-trial EEG dynamics including independent component analysis. J Neurosci Methods 134, 9–21. https://doi.org/10.1016/j.jneumeth.2003.10.009

Dentico, D., Ferrarelli, F., Riedner, B.A., Smith, R., Zennig, C., Lutz, A., Tononi, G., Davidson, R.J., 2016. Short Meditation Trainings Enhance Non-REM Sleep Low-Frequency Oscillations. PLoS One 11. https://doi.org/10.1371/JOURNAL.PONE.0148961

Esser, S.K., Hill, S.L., Tononi, G., 2007. Sleep homeostasis and cortical synchronization: I. Modeling the effects of synaptic strength on sleep slow waves. Sleep 30, 1617–1630. https://doi.org/10.1093/SLEEP/30.12.1617

Ferrarelli, F., Smith, R., Dentico, D., Riedner, B.A., Zennig, C., Benca, R.M., Lutz, A., Davidson, R.J., Tononi, G., 2013. Experienced mindfulness meditators exhibit higher parietal-occipital EEG gamma activity during NREM sleep. PLoS One 8. https://doi.org/10.1371/JOURNAL.PONE.0073417

Giedd, J.N., Blumenthal, J., Jeffries, N.O., Rajapakse, J.C., Vaituzis, A.C., Liu, H., Berry, Y.C., Tobin, M., Nelson, J., Castellanos, F.X., 1999. Development of the human corpus callosum during childhood and adolescence: a longitudinal MRI study. Prog Neuropsychopharmacol Biol Psychiatry 23, 571–588. https://doi.org/10.1016/S0278-5846(99)00017-2

Gogtay, N., Giedd, J.N., Lusk, L., Hayashi, K.M., Greenstein, D., Vaituzis, A.C., Nugent, T.F., Herman, D.H., Clasen, L.S., Toga, A.W., Rapoport, J.L., Thompson, P.M., 2004. Dynamic mapping of human cortical development during childhood through early adulthood. Proc Natl Acad Sci U S A 101, 8174–8179. https://doi.org/10.1073/PNAS.0402680101

Gorgoni, M., D'Atri, A., Scarpelli, S., Reda, F., de Gennaro, L., 2020. Sleep electroencephalography and brain maturation: developmental trajectories and the relation with cognitive functioning. Sleep Med 66, 33–50. https://doi.org/10.1016/J.SLEEP.2019.06.025

Haxby, J. v., Guntupalli, J.S., Connolly, A.C., Halchenko, Y.O., Conroy, B.R., Gobbini, M.I., Hanke, M., Ramadge, P.J., 2011. A common, high-dimensional model of the representational space in human ventral temporal cortex. Neuron 72, 404–416. https://doi.org/10.1016/J.NEURON.2011.08.026

Jenni, O.G., Carskadon, M.A., 2004. Spectral analysis of the sleep electroencephalogram during adolescence. Sleep 27, 774–783. https://doi.org/10.1093/sleep/27.4.774

Jolles, D.D., van Buchem, M.A., Crone, E.A., Rombouts, S.A.R.B., 2011. A comprehensive study of whole-brain functional connectivity in children and young adults. Cereb Cortex 21, 385–391. https://doi.org/10.1093/CERCOR/BHQ104

Kelly, A.M.C., di Martino, A., Uddin, L.Q., Shehzad, Z., Gee, D.G., Reiss, P.T., Margulies, D.S., Castellanos, F.X., Milham, M.P., 2009. Development of anterior cingulate functional connectivity from late childhood to early adulthood. Cereb Cortex 19, 640–657. https://doi.org/10.1093/CERCOR/BHN117

Keshavan, M.S., Diwadkar, V.A., DeBellis, M., Dick, E., Kotwal, R., Rosenberg, D.R., Sweeney, J.A., Minshew, N., Pettegrew, J.W., 2002. Development of the corpus callosum in childhood, adolescence and early adulthood. Life Sci 70, 1909–1922. https://doi.org/10.1016/S0024-3205(02)01492-3

Kurth, S., Achermann, P., Rusterholz, T., Lebourgeois, M.K., 2013. Development of Brain EEG Connectivity across Early Childhood: Does Sleep Play a Role? Brain Sci 3, 1445–1460. https://doi.org/10.3390/BRAINSCI3041445

Kurth, S., Riedner, B.A., Dean, D.C., O'Muircheartaigh, J., Huber, R., Jenni, O.G., Deoni, S.C.L., LeBourgeois, M.K., 2017. Traveling Slow Oscillations During Sleep: A Marker of Brain Connectivity in Childhood. Sleep 40. https://doi.org/10.1093/SLEEP/ZSX121

Kurth, S., Ringli, M., Geiger, A., Lebourgeois, M., Jenni, O.G., Huber, R., 2010. High-Density Sleep Electroencephalogram Study. Journal of Neuroscience 30, 13211–13219. https://doi.org/10.1523/JNEUROSCI.2532-10.2010.Mapping

Kurth, S., Ringli, M., LeBourgeois, M.K., Geiger, A., Buchmann, A., Jenni, O.G., Huber, R., 2012. Mapping the electrophysiological marker of sleep depth reveals skill maturation in children and adolescents. Neuroimage 63, 959–965. https://doi.org/10.1016/J.NEUROIMAGE.2012.03.053

Lee, G.M.H., Fattinger, S., Mouthon, A.L., Noirhomme, Q., Huber, R., 2013. Electroencephalogram approximate entropy influenced by both age and sleep. Front Neuroinform 7. https://doi.org/10.3389/FNINF.2013.00033

Lopez-Larson, M.P., Anderson, J.S., Ferguson, M.A., Yurgelun-Todd, D., 2011. Local brain connectivity and associations with gender and age. Dev Cogn Neurosci 1, 187–197. https://doi.org/10.1016/J.DCN.2010.10.001

Luders, E., Cherbuin, N., Thompson, P.M., Gutman, B., Anstey, K.J., Sachdev, P., Toga, A.W., 2010a. When more is less: Associations between corpus callosum size and handedness lateralization. Neuroimage 52, 43–49. https://doi.org/10.1016/J.NEUROIMAGE.2010.04.016

Luders, E., Thompson, P.M., Toga, A.W., 2010b. The development of the corpus callosum in the healthy human brain. J Neurosci 30, 10985–10990. https://doi.org/10.1523/JNEUROSCI.5122-09.2010

Lynch, K.M., Cabeen, R.P., Toga, A.W., Clark, K.A., 2020. Magnitude and timing of major white matter tract maturation from infancy through adolescence with NODDI. Neuroimage 212, 116672. https://doi.org/10.1016/J.NEUROIMAGE.2020.116672

Mascetti, G.G., 2016. Unihemispheric sleep and asymmetrical sleep: behavioral, neurophysiological, and functional perspectives. Nat Sci Sleep 8, 221. https://doi.org/10.2147/NSS.S71970

Massimini, M., Huber, R., Ferrarelli, F., Hill, S., Tononi, G., 2004. The sleep slow oscillation as a traveling wave. J Neurosci 24, 6862–6870. https://doi.org/10.1523/JNEUROSCI.1318-04.2004

Maureen, C., 2010. An empirical evaluation of free BEM solvers for accurate M/EEG forward modeling. Front Neurosci. https://doi.org/10.3389/conf.fnins.2010.06.00065

Menicucci, D., Piarulli, A., Debarnot, U., d'Ascanio, P., Landi, A., Gemignani, A., 2009. Functional structure of spontaneous sleep slow oscillation activity in humans. PLoS One 4. https://doi.org/10.1371/JOURNAL.PONE.0007601

Mensen, A., Riedner, B., Tononi, G., 2016. Optimizing detection and analysis of slow waves in sleep EEG. J Neurosci Methods 274, 1–12. https://doi.org/10.1016/J.JNEUMETH.2016.09.006

Miano, S., Amato, N., Foderaro, G., Pezzoli, V., Ramelli, G.P., Toffolet, L., Manconi, M., 2019. Sleep phenotypes in attention deficit hyperactivity disorder. Sleep Med 60, 123–131. https://doi.org/10.1016/j.sleep.2018.08.026

Murphy, M., Riedner, B.A., Huber, R., Massimini, M., Ferrarelli, F., Tononi, G., 2009. Source modeling sleep slow waves. Proc Natl Acad Sci U S A 106, 1608–1613. https://doi.org/10.1073/pnas.0807933106

Nichols, T.E., Holmes, A.P., 2002. Nonparametric permutation tests for functional neuroimaging: a primer with examples. Hum Brain Mapp 15, 1–25. https://doi.org/10.1002/HBM.1058

Novelli, L., D'atri, A., Marzano, C., Finotti, E., Ferrara, M., Bruni, O., De Gennaro, L., 2016. Mapping changes in cortical activity during sleep in the first 4 years of life. J Sleep Res 25, 381–389. https://doi.org/10.1111/JSR.12390

Pascual-Marqui, R.D., 2002. Standardized low-resolution brain electromagnetic tomography (sLORETA): Technical details, in: Methods and Findings in Experimental and Clinical Pharmacology.

Paus, T., 2005. Mapping brain maturation and cognitive development during adolescence. Trends Cogn Sci 9, 60–68. https://doi.org/10.1016/J.TICS.2004.12.008

Paus, T., Keshavan, M., Giedd, J.N., 2008. Why do many psychiatric disorders emerge during adolescence? Nat Rev Neurosci 9, 947–957. https://doi.org/10.1038/NRN2513

Piekarski, D.J., Johnson, C.M., Boivin, J.R., Thomas, A.W., Lin, W.C., Delevich, K., Galarce, E.M., Wilbrecht, L., 2017. Does puberty mark a transition in sensitive periods for plasticity in the associative neocortex? Brain Res 1654, 123. https://doi.org/10.1016/J.BRAINRES.2016.08.042

Rajapakse, J.C., Giedd, J.N., Rumsey, J.M., Vaituzis, A.C., Hamburger, S.D., Rapoport, J.L., 1996. Regional MRI measurements of the corpus callosum: A methodological and developmental study. Brain Dev 18, 379–388. https://doi.org/10.1016/0387-7604(96)00034-4

Ricci, A., He, F., Fang, J., Calhoun, S.L., Vgontzas, A.N., Liao, D., Younes, M., Bixler, E.O., Fernandez-Mendoza, J., 2021. Maturational trajectories of non-rapid eye movement slow wave activity and odds ratio product in a population-based sample of youth. Sleep Med 83, 271–279. https://doi.org/10.1016/J.SLEEP.2021.05.002

Richards, J.E., Sanchez, C., Phillips-Meek, M., Xie, W., 2016. A database of age-appropriate average MRI templates. Neuroimage. https://doi.org/10.1016/j.neuroimage.2015.04.055

Riedner, B.A., Vyazovskiy, V. v., Huber, R., Massimini, M., Esser, S., Murphy, M., Tononi, G., 2007. Sleep homeostasis and cortical synchronization: III. A high-density EEG study of sleep slow waves in humans. Sleep 30, 1643–1657. https://doi.org/10.1093/sleep/30.12.1643

Ringli, M., Huber, R., 2011. Developmental aspects of sleep slow waves: linking sleep, brain maturation and behavior. Prog Brain Res 193, 63–82. https://doi.org/10.1016/B978-0-444-53839-0.00005-3

Schoch, S.F., Riedner, B.A., Deoni, S.C., Huber, R., Lebourgeois, M.K., Kurth, S., 2018. Across-night dynamics in traveling sleep slow waves throughout childhood. Sleep 41. https://doi.org/10.1093/sleep/zsy165

Shaw, P., Kabani, N.J., Lerch, J.P., Eckstrand, K., Lenroot, R., Gogtay, N., Greenstein, D., Clasen, L., Evans, A., Rapoport, J.L., Giedd, J.N., Wise, S.P., 2008. Neurodevelopmental trajectories of the human cerebral cortex. J Neurosci 28, 3586–3594. https://doi.org/10.1523/JNEUROSCI.5309-07.2008

Siclari, F., Bernardi, G., Riedner, B.A., LaRocque, J.J., Benca, R.M., Tononi, G., 2014. Two distinct synchronization processes in the transition to sleep: A high-density electroencephalographic study. Sleep 37, 1621-1637F. https://doi.org/10.5665/sleep.4070

Spiess, M., Bernardi, G., Kurth, S., Ringli, M., Wehrle, F.M., Jenni, O.G., Huber, R., Siclari, F., 2018. How do children fall asleep? A high-density EEG study of slow waves in the transition from wake to sleep. Neuroimage 178, 23–35. https://doi.org/10.1016/j.neuroimage.2018.05.024

Tamaki, M., Bang, J.W., Watanabe, T., Sasaki, Y., 2016. Night watch in one brain hemisphere during sleep associated with the first-night effect in humans. Curr Biol 26, 1190. https://doi.org/10.1016/J.CUB.2016.02.063

Thompson, P.M., Gledd, J.N., Woods, R.P., MacDonald, D., Evans, A.C., Toga, A.W., 2000. Growth patterns in the developing brain detected by using continuum mechanical tensor maps. Nature 2000 404:6774 404, 190–193. https://doi.org/10.1038/35004593

Timofeev, I., Schoch, S.F., LeBourgeois, M.K., Huber, R., Riedner, B.A., Kurth, S., 2020. Spatio-temporal properties of sleep slow waves and implications for development. Curr Opin Physiol 15, 172–182. https://doi.org/10.1016/J.COPHYS.2020.01.007

Tzourio-Mazoyer, N., Landeau, B., Papathanassiou, D., Crivello, F., Etard, O., Delcroix, N., Mazoyer, B., Joliot, M., 2002. Automated anatomical labeling of activations in SPM using a macroscopic anatomical parcellation of the MNI MRI single-subject brain. Neuroimage. https://doi.org/10.1006/nimg.2001.0978

Vyazovskiy, V. v., Riedner, B.A., Cirelli, C., Tononi, G., 2007. Sleep homeostasis and cortical synchronization: II. A local field potential study of sleep slow waves in the rat. Sleep 30, 1631–1642. https://doi.org/10.1093/SLEEP/30.12.1631

Westerhausen, R., Fjell, A.M., Krogsrud, S.K., Rohani, D.A., Skranes, J.S., Håberg, A.K., Walhovd, K.B., 2016. Selective increase in posterior corpus callosum thickness between the age of 4 and 11 years. Neuroimage 139, 17–25. https://doi.org/10.1016/J.NEUROIMAGE.2016.06.008

Data and code availability statements

Data and code are only available on request via a formal request to the corresponding authors due to the need for a formal data sharing agreement.